



# Design and Analysis of a Novel Horizontal Large-Amplitude and Low-Frequency Vibration Isolator

Shuai Wang<sup>1</sup> · Lang Yu<sup>1</sup> · Qinghua Zhang<sup>2,3</sup> · Rui Xiang<sup>4</sup>

Received: 9 August 2023 / Revised: 24 November 2023 / Accepted: 27 November 2023 / Published online: 2 January 2024  
© Springer Nature Singapore Pte Ltd. 2024

## Abstract

**Purpose** This paper proposes a novel dual four-rod horizontal large-amplitude quasi-zero stiffness (QZS) vibration isolator based on the singular configuration of a planar four-rod mechanism combined with gravity compensation.

**Methods** First, the mechanism design and three-dimensional model of dual four-rod horizontal vibration isolator are established. Second, kinematic characteristics are analyzed, and trajectory planning is carried out to obtain the kinematic performance. Then, based on the artificial fish swarm algorithm, the appropriate size and mass of the component are solved, and the QZS characteristics of the isolator are optimized. Third, the statics and dynamics theoretical models of isolators are established, and the transmissibility of isolators under different damping ratios and excitation amplitudes is solved by simulation experiments. Finally, the experimental prototype is established, and the experiment of resilience and acceleration transmissibility is carried out to verify the effectiveness of low-frequency vibration isolation.

**Results** The static and dynamic simulation analysis of isolator well verifies the theoretical solution of isolator. According to the theoretical model, different vibration isolation performance can be obtained with different input parameters. The experimental results of the prototype show that the isolator has lower initial vibration isolation frequency and wider vibration isolation bandwidth.

**Conclusion** The dual four-rod horizontal large-amplitude QZS isolator designed in this paper shows good performance in isolating the external excitation of the low-frequency large vibration amplitude. Since the medical precision instrument will inevitably produce low-frequency vibration during the transportation process and reduce the accuracy and stability of the equipment, in order to reduce the possibility of the instrument being damaged during the transportation process, the vibration isolator has great application potential in the isolation of medical precision instrument.

**Keywords** Horizontal low-frequency vibration isolation · Singular mechanism · Quasi-zero stiffness · Trajectory optimization

✉ Qinghua Zhang  
doctorzhangqinghua@163.com

<sup>1</sup> Department of Mechanical Engineering, Dongguan University of Technology, Dongguan 523808, China

<sup>2</sup> Department of Neurosurgery, Huazhong University of Science and Technology Union Shenzhen Hospital, Shenzhen 518052, Guangdong, China

<sup>3</sup> The 6, Affiliated Hospital of Shenzhen University Health Science Center, Shenzhen, Guangdong, China

<sup>4</sup> Department of Geriatrics, The Ninth Hospital of Xi'an Affiliated Hospital of Xi'an Jiaotong University, Xi'an, Shanxi, China

## Introduction

Vibration is ubiquitous in engineering applications such as construction machinery, aerospace, vehicles, and precision devices [1]. Adverse vibration may affect the normal function of precision devices and even cause large deformations and damage to the mechanical structure. Therefore, it is necessary to isolate and suppress harmful vibration and control it within a reasonable and acceptable range to avoid large economic losses and resource waste [2].

There is a contradiction between the bearing capacity and vibration isolation performance of traditional linear vibration isolation systems. Normally, when the external excitation frequency is greater than  $\sqrt{2}$  times the natural frequency of the system, the linear isolator can work effectively [3–5].

Therefore, its performance is superior in high-frequency vibration isolation, but it is difficult to achieve low-frequency vibration isolation. Thus, the nonlinear vibration isolator is proposed to solve the problem of low-frequency vibration isolation [6]. When vibration isolator vibrates near the operating point, its dynamic stiffness is close to 0, this kind of vibration isolator is called QZS vibration isolator. The QZS vibration isolator has high static stiffness and low dynamic stiffness, which can withstand a large mass load and a large range of vibration isolation. It can also solve the problem of low-frequency vibration isolation and large displacement conflict when using a linear vibration isolator [7, 8]. The QZS vibration isolator has sufficient static stiffness to reduce static load and, at the same time, provides low dynamic stiffness near the equilibrium position for vibration isolation [9–11]. Such so-called static high stiffness and dynamic low stiffness characteristics enable the QZS isolator to work at a low external excitation frequency [12, 13]. The characteristics of QZS vibration isolator are usually obtained by parallel connections of positive and negative stiffness [14–16].

Alabuzhev et al. first proposed the concept of QZS, introduced negative stiffness mechanism into linear vibration isolation system, and defined the QZS theory for the first time [17]. Carrella et al. constructed a new QZS vibration isolation mechanism consisting of three springs using inclined springs as negative stiffness elements [18, 19]. Kovacic et al. adopted preloaded nonlinear spring instead of linear spring to solve the problem of drastic changes in dynamic stiffness after the system deviates from the equilibrium position [20]. Zhou et al. proposed a cam-spring mechanism. The research shows that no matter what the excitation amplitude of the vibration isolation system is the peak transfer rate and initial frequency of the vibration isolation are not higher than that of the corresponding linear isolator, which realizes the structural innovation of the negative stiffness mechanism [21]. Kim et al. proposed a QZS vibration isolator composed of a vertical spring with preload and eight transverse leaf springs with nonlinear buckling characteristics [22]. Dalela et al. used a bistable cosine beam instead of a nonlinear inclined spring as a negative stiffness mechanism to design a vertical vibration isolation system with single degrees of freedom [23]. Zhang et al. designed a new QZS torsional vibration isolator to adapt to load changes by adjusting positive stiffness and synchronously adjusting negative stiffness so that the vibration isolator would always work in the QZS state, aiming at the problem that the existing QZS torsional vibration isolator is only applicable to constant load [24]. In addition, there are negative stiffness mechanisms designed by combining Euler buckling beam [25, 26], air spring [27], composite structure [28–30] and bionic structure [31–33], etc., which greatly increase the types and number of QZS vibration isolators. However, the design of these vibration

isolators still has some defects in compactness and structural stability, which need be further developed.

In this paper, a QZS isolator with a simple and compact structure that can achieve low frequency and heavy load vibration isolation in the horizontal direction is designed. For the realization of QZS, the special structure of plane four-rod mechanism is adopted to realize the horizontal QZS, which has the advantages of simple structure and compact structure compared with the traditional spring structure vibration isolator. In vibration isolation systems, the dual four-rod structure consists of simple basic mechanical elements, rods and hinges that provide reliable QZS near the equilibrium position. In addition, in terms of achieving QZS isolation, the isolator can achieve a wide range of horizontal low-frequency vibration isolation and the load can be borne by two sets of four-rod mechanisms in practical applications. Therefore, the vibration isolator can realize vibration isolation for large loads without increasing the structure of the vibration isolator, which makes it have greater application potential. The dual four-rod isolators offer further improvements in simplicity and compactness compared to previous isolators, and are more suitable for heavy load isolation requirements. In “[Conceptual Design and Parameter Optimization](#)”, the conceptual design and physical model of the new dual four-rod vibration isolator are presented, and the parameter design and optimization of QZS are carried out. In “[Mechanical analysis of the vibration isolator](#)”, the dynamic model of the new dual four-rod isolator is established, and the theoretical isolation performance of the isolator is simulated. In “[Experimental Validation](#)”, experimental platforms are established, and static and dynamic tests are performed. The vibration isolation effect in “[Conclusions](#)” is evaluated. Finally, Sect. 5 ends the paper with conclusions and remarks.

## Conceptual Design and Parameter Optimization

In this section, the dual four-rod vibration isolator is physically modeled and analyzed, the motion trajectory of the isolator is planned, and the motion trajectory of the isolator working platform is realized as a horizontal quasi-straight line. By optimizing the member center of mass, the isolator equivalent center of mass is realized without deviation near the equilibrium position, which simplifies the motion analysis process. The specific contents are as follows.

### Vibration Isolator Structure Design

Figure 1 shows the proposed the dual four-rod QZS vibration isolator model. The model of the vibration isolator is a central symmetrical structure. The main structure of the

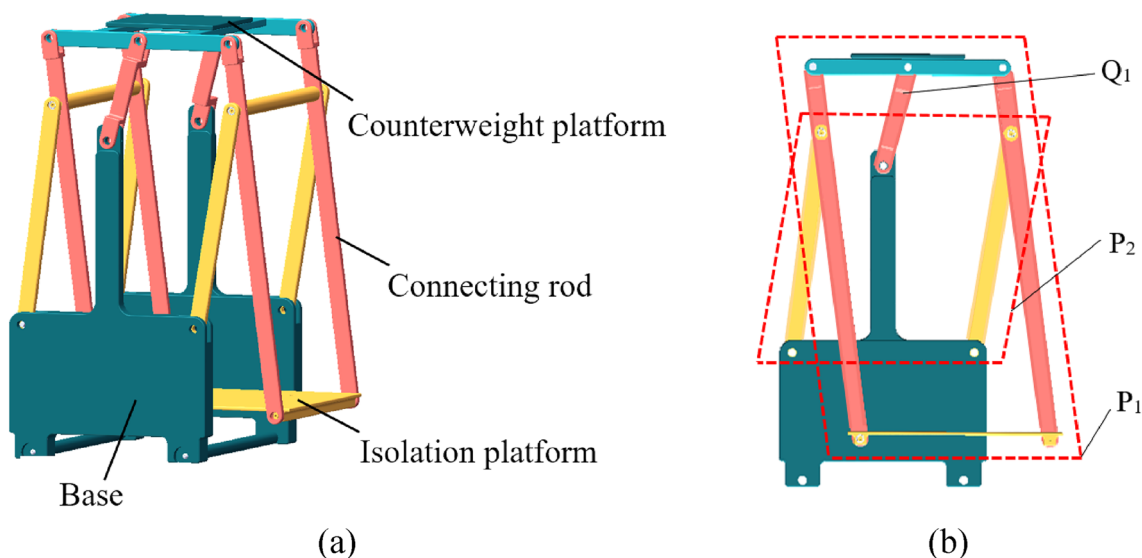


**Fig. 1** Dual four-rod horizontal vibration isolator. **a** Three-dimensional model of the vibration isolator, **b** schematic diagram of the unilateral structure

vibration isolator can be divided into three parts.  $P_1$  is the first set of parallelogram structure for the vibration isolator, which are hinged to the upper counterweight platform and the lower vibration isolator platform by a long connecting rod.  $P_2$  is the second parallelogram structure of the isolator, which is hinged to  $P_1$  and the base, respectively. The middle swing rod is hinged with the upper counterweight platform and the lower base, respectively.

The vibration isolator model proposed in this paper is centrosymmetric, and there are many rods with the same function. In order to simplify the calculation, the rods with the same motion are treated as equivalent, where  $Q_1$  and  $P_2$  are hinged with the base, and the motion track of the upper end of both is an arc, which jointly provides the supporting force of  $P_1$ .  $Q_1$  can be simplified to  $CD$ ,  $P_2$  to  $OA$ , and  $P_1$  to  $CB$ . The connection part between the upper end  $OF$  of the  $P_2$  rod and the  $P_1$  rod can be simplified as  $OF$ , and the connection part between the counterweight platform and  $Q_1$  can be simplified as  $DE$ . The simplified equivalent mechanism diagram of the vibration isolator is obtained, as shown in Fig. 2.  $OD$  is a part of the base.  $B$  is a vibration isolation platform. Assume that the mass of the object to be isolated is  $M$ . The lengths of each member are  $OA = l_1$ ,  $CD = l_3$ ,  $OD = l_4$ ,  $AB = d_1$ ,  $AC = d_2$ , respectively. Rods  $OA$  and  $CD$  rotate around points  $O$  and  $D$ , respectively, and rods  $BC$  and rods  $OA$  and  $CD$  are connected by hinges at points  $A$  and  $C$ , respectively.

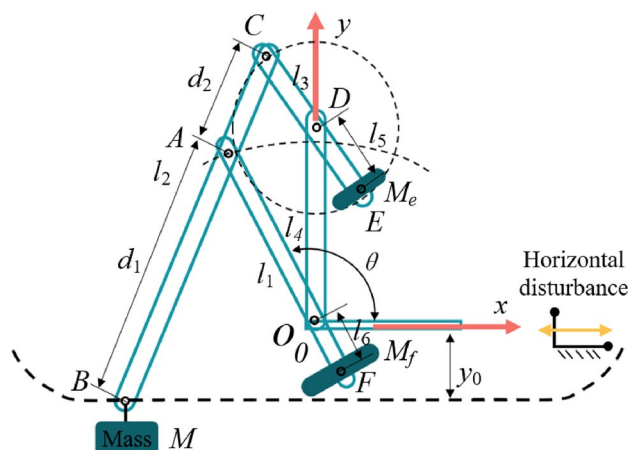


**Fig. 2** Schematic diagram of the vibration isolator mechanism

### Trajectory Planning of Working Platform

In order to make the movement of the working platform symmetrical with respect to the  $OD$  rod and the mechanism can produce a singular increase in the degree of freedom at the central equilibrium position, the length of each rod must satisfy

$$l_1 + d_2 = l_4 + l_3. \tag{1}$$

As shown in Fig. 2, point  $O$  is selected as the origin to establish the coordinate system.  $A$  and  $C$  move in a circle around  $O$  and  $D$ , respectively. According to the law of circular motion, we can obtain

$$\begin{cases} (x_C - x_A)^2 + (y_C - y_A)^2 = d_2^2 \\ (x_C - x_D)^2 + (y_C - y_D)^2 = (l_3)^2 \end{cases}, \quad (2)$$

$\overline{AB}$  and  $\overline{CA}$  are collinear, and there is  $\overline{AB} = \frac{d_1}{d_2} \overline{CA}$ . The relationship equation between point  $B$  and points  $A$  and  $C$  are established as

$$\begin{cases} x_B = \frac{d_1}{d_2}(x_A - x_C) + x_A \\ y_B = \frac{d_1}{d_2}(y_A - y_C) + y_A \end{cases}. \quad (3)$$

The coordinates of point  $B$  can be obtained by Eqs. (2) and (3) as

$$\begin{cases} x_B = l_1 \cos(\theta) + \frac{d_1 Q}{d_2} \\ y_B = l_1 \sin(\theta) - \frac{d_1 \sqrt{d_2^2 + l_1^2 \cos^2(\theta)} - S \sqrt{d_2^2 - l_1^2 \cos^2(\theta)} + S}{d_2} \end{cases}. \quad (4)$$

Here,

$$Q = l_1 \cos(\theta) - \frac{l_1^3 \cos(\theta) + \text{sign}\left(\frac{\pi}{2} - \theta\right) R l_4 - d_2^2 l_1 \cos(\theta) + l_1 l_3^2 \cos(\theta)}{2l_1^2 + 2l_4^2 - 4l_1 l_4 \sin(\theta)} + \frac{l_1 l_4^2 \cos(\theta) - \text{sign}\left(\frac{\pi}{2} - \theta\right) R l_1 \sin(\theta) - 2l_1^2 l_4 \cos(\theta) \sin(\theta)}{2l_1^2 + 2l_4^2 - 4l_1 l_4 \sin(\theta)},$$

$$R = (2d_2^2 l_1^2 - l_1^4 - l_3^4 - l_4^4 - d_2^4 + 2d_2^2 l_3^2 + 2d_2^2 l_4^2 + 2l_1^2 l_3^2 - 2l_1^2 l_4^2 + 2l_3^2 l_4^2 - 4l_1^2 l_4^2 \sin^2(\theta) + 4l_1 l_3^2 \sin(\theta) + 4l_1^3 l_4 \sin(\theta) - 4d_2^2 l_1 l_4 \sin(\theta) - 4l_1 l_3^2 l_4 \sin(\theta))^{\frac{1}{2}},$$

$$S = \frac{l_1^3 \cos(\theta) + \text{sign}\left(\frac{\pi}{2} - \theta\right) R l_4 - d_2^2 l_1 \cos(\theta) + l_1 l_3^2 \cos(\theta)}{2l_1^2 + 2l_4^2 - 4l_1 l_4 \sin(\theta)} + \frac{l_1 l_4^2 \cos(\theta) - \text{sign}\left(\frac{\pi}{2} - \theta\right) R l_1 \sin(\theta) - 2l_1^2 l_4 \cos(\theta) \sin(\theta)}{2l_1^2 + 2l_4^2 - 4l_1 l_4 \sin(\theta)}.$$

## Motion Trajectory and QZS Optimization

The motion trajectory of the vibration isolation platform is complicated, and there are many parameters affecting its motion. There are countless groups of rod lengths meeting the requirements when solving the ideal trajectory only through the equation, and all rod lengths can be scaled in the same proportion, and there will be more rod length combinations meeting the accuracy conditions. The coordinate expressions of  $B$  and  $C$  obtained in the above kinematic analysis are highly nonlinear equations, so it is difficult to search the optimal solution by conventional calculation or gradient method. Artificial fish swarm algorithm (AFSA) is not sensitive to the initial value, has low requirements on the

objective function and has the ability to obtain the optimal solution globally.

## Motion Trajectory Optimization

The individual state of artificial fish can be represented by vector  $X = (x_1, x_2, \dots, x_n)$ , while  $x_i$  ( $i = 1, 2, \dots, n$ ) is an artificial fish in path optimization, and the population size of artificial fish is  $N$ . The food concentration at the current position of artificial fish can be expressed as  $Y = f(x)$ ,  $\delta$  is the crowding factor,  $t$  is the number of iterations,  $Step$  is the moving step length of artificial fish, and  $\text{Rand}(0, 1)$  is the random number of  $(0, 1)$ .

This paper mainly adopts the clustering behavior of fish schools to optimize. Assume the number  $N$  of artificial fish in the current artificial fish  $X_i$  neighborhood and its center position  $X_B$ . If  $\delta Y_i < Y_B/N$  indicates that the center of the artificial fish in the neighborhood is not too crowded and the food concentration is relatively high, then move one unit step toward  $X_B$  through Eq. (5), otherwise perform foraging behavior:

$$X_i(t+1) = X_i(t) + \frac{X_B(t) - X_i(t)}{\|X_B(t) - X_i(t)\|} \times \text{Step} \times \text{Rand}(0, 1). \quad (5)$$

According to the principle of fish swarm algorithm, the angle  $\theta$  of connecting rod  $OA$  around the base is taken as the independent variable, and the longitudinal expression of point  $B$  is set as  $f_y(\theta) = y_B$ . In the whole interval, the motion trajectory of point  $B$  is continuously derivable, and  $y_B$  obtains the minimum value  $y_{\min} = l_1 - d_1$  when the center position is required. The movement range of point  $B$  in the abscissa direction is related to the size of the vibration isolation interval. Let the abscissa expression of point  $B$  be  $f_x(\theta) = x_B$ , and define the horizontal movement interval as  $[-L_k, L_k]$ .

According to  $f_y(\theta)$  monotonicity, minimum value, and  $f_x(\theta)$  maximum motion interval, the basic constraints can be obtained:

$$\begin{cases} f_y(\theta)_{\min} = l_1 - d_1, \theta = \frac{\pi}{2} \\ f_y'(\theta) \leq 0, \theta \in \left[\frac{\pi}{2} + \frac{\pi}{20}, \frac{\pi}{2}\right] \\ f_y'(\theta) \geq 0, \theta \in \left[\frac{\pi}{2}, \frac{\pi}{2} - \frac{\pi}{20}\right] \\ f_x(\theta)_{\max} \geq L_k, \theta \in \left(\frac{\pi}{2}, \frac{\pi}{2} - \frac{\pi}{20}\right) \end{cases}. \quad (6)$$

That is, search and obtain the combination of rod length with the minimum fluctuation of the ordinate of point  $B$  within the given range of motion, and the corresponding expression is

$$g_{\text{opt}}(\theta) \rightarrow \min. \tag{7}$$

Considering the structural size of the vibration isolator and subsequent processing conditions, we define  $l_1 = 0.35$  m, the rod length range of  $d_1, l_3, l_4$  is [0.05 m, 1 m], the rod length range of  $d_2$  is [0.1 m, 1.5 m], and the ordinate of the vibration isolation point  $B$  allows the maximum. The fluctuation value is set to  $\delta < 0.5$  mm and some intervals are discarded in advance.

The search optimization convergence process is shown in Fig. 3. After 1349 optimizations, the target value is within 0.05 to meet the design requirements. For the convenience of subsequent analysis and combined with the processing and assembly conditions, the length of each rod is selected under the condition of satisfying the error accuracy, as shown in Table 1.

Substitute length data of the optimized pole into the Eq. (4) to select  $\theta \in \left[ \frac{9\pi}{20}, \frac{11\pi}{20} \right]$ , and evenly select 50 values in the interval to draw and draw the motion track points of the working platform, and the fitting curve is  $y(x) = 0.3946x^4 - 0.1382$ . From Fig. 4, it can be seen that the movement trajectory of the working platform in a relatively large range in the horizontal direction is a quasi-straight line.

### QZS Optimization

The motion trajectory optimization ensures that the motion trajectory of the vibration isolator working platform is quasi-straight line. If the mass of the rod itself is not considered, the system has achieved QZS. However, as the input angle  $\theta$  changes, the accompanying motion of each member will cause its comprehensive center of gravity to change in the vertical direction. For low-frequency vibration isolation, the influence of the load and the gravity generated by its own

**Table 1** Quasi-straight line optimization results

Lever	Results (m)	Length	Results (m)
$l_1$	0.350	$d_1$	0.48825
$l_3$	0.16034	$d_2$	0.105
$l_4$	0.29471		

structure on the total stiffness of the system must be considered. This type of vibration isolator based on the principle of a single pendulum needs to minimize the impact of load mass on the performance of the isolation mechanism, and the change in gravitational potential energy of the isolation mechanism itself during movement. The ideal situation is that the overall height of the center of gravity of the mechanism is always constant.

Rods  $OA$  and  $CD$  rotate around points  $O$  and  $D$ , respectively. If the two rods are doubled in the other direction, their center of mass can remain unchanged during the motion. The rod  $OD$  is fixed, and its center of mass does not change during the movement. For the rod  $BC$ , its motion is a compound motion of rotation and movement, and the trajectory of the center of mass is complex. In order to simplify the problem, taking the center of mass of the base rod  $OD$  as the reference object, add counterweights  $M_e$  and  $M_f$  to the reverse extension lines of the rods  $OA$  and  $CD$ , respectively, assuming that the mass of all rods is uniformly distributed and the mass is only related to the length. Let the linear density be  $\rho_0$ , and express the mass at points  $E$  and  $F$  as

$$\begin{cases} M_e = \rho_0 l_e \\ M_f = \rho_0 l_f \end{cases} \tag{8}$$

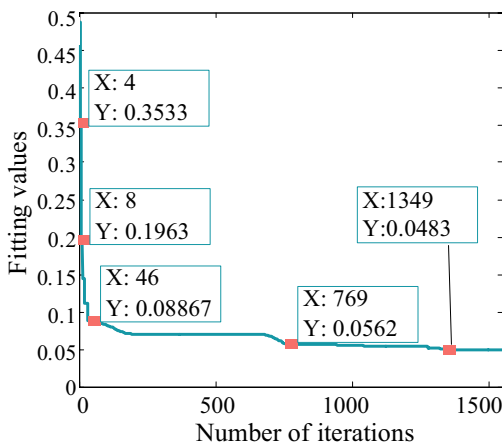


**Fig. 3** Optimizing tracking process curve

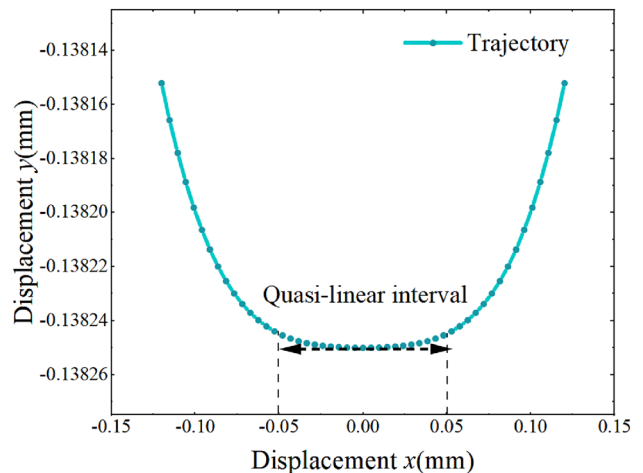


**Fig. 4** Motion trajectory fitting curve of the working platform

Then, the vertical coordinates of the combined equivalent centroid of each active member and counterweight  $M_e$  and  $M_f$  is

$$\bar{y}(\theta) = \frac{1}{2} \frac{(y_B + y_C)l_2 + y_D l_4 + y_E l_5 + y_F l_6 + 2y_E l_e + 2y_F l_f}{l_2 + l_4 + l_5 + l_6 + l_e + l_f} \tag{9}$$

In order to ensure the stability of the vibration isolator system, the comprehensive equivalent centroid height  $\bar{h}_y$  of the system is the smallest when it is at the center equilibrium position and has a monotonous increase when it deviates from the central position. The constraints of the comprehensive centroid are

$$\begin{cases} \bar{y}(\theta)_{\min} = \bar{h}_y, \theta = \frac{\pi}{2} \\ \bar{y}'(\theta) \leq 0, \theta \in \left[ \frac{\pi}{2} + \frac{\pi}{20}, \frac{\pi}{2} \right) \\ \bar{y}'(\theta) \geq 0, \theta \in \left( \frac{\pi}{2}, \frac{\pi}{2} - \frac{\pi}{20} \right] \end{cases} \tag{10}$$

Setting the constraint conditions of each rod as  $l_5 \in (0, 0.16)$ ,  $l_6 \in (0, 0.35)$ , the counterweight mass  $l_e \in (0, 30)$ ,  $l_f \in (0, 30)$ , and set the linear density as  $\rho_0 = 4.83 \text{ kg/m}$ . The design objective equation is

$$h_{\text{opt}}(\theta) = \bar{y}(\theta) - \bar{h}_y \tag{11}$$

Similarly, AFSA was used to find the optimal solution. After 800 iterations, a stable optimal solution was found at the 301st. The weight optimization results are shown in Table 2.

According to the optimized structural parameters and mass parameters of the counterweight, the mass of the vibration isolation mechanism itself is 24.56 kg. The trajectory of the vibration isolator working platform is curve-fitted to obtain the trajectory equation as  $y(x) = 0.3946x^4 - 0.1382$ .

### Mechanical Analysis of the Vibration Isolator

In this section, the stiffness of the isolator is analyzed theoretically, and QZS can be obtained near the equilibrium position. The dynamic model of the dual four-rod horizontal vibration isolator is established. The dynamic response

**Table 2** QZS optimization parameter results

Lever	Results (m)	Quality	Results (kg)
$l_5$	0.01115	$M_e$	3.4654
$l_6$	0.10525	$M_f$	4.8144
$l_e$	0.71748	–	–
$l_f$	0.99678	–	–

of the isolator is solved by polynomial fitting and the harmonic balance method. By studying the influence of different parameters on the displacement transmissibility, the vibration isolation performance of the isolator is studied and explained.

### Stiffness Analysis

As shown in Fig. 5, the motion of the vibration isolated object on the working platform is equivalent to the motion along the track with the fitting curve as the contour. The force analysis model of a vibration isolated object, where  $y(x)$  is the trajectory equation of the vibration isolated object,  $y'(x_i, y_i)$  is the slope of the tangent line of the center of mass of the vibration isolated object on the trajectory;  $\beta$  is the angle between the tangent line and the abscissa,  $M$  is the mass of the vibration isolated object, and  $F_N$  is the orbit pair. The supporting force of the vibration isolated object  $F_H$  is the horizontal component force of the vibration isolated object.

The initial state of the vibration isolated object is in the static equilibrium position. The centroid position equation of the vibration isolated object is  $M_{(x_i, y_i)}$ , and the motion trajectory equation is  $y(x)$ . According to the motion path of the isolated object, the tangent equation at its centroid is obtained:

$$y(x) = y'_{(x_i, y_i)}(x - x_i) + y_i \tag{12}$$

The origin of the coordinates is established at the midpoint of the trajectory, the vibration isolated object is on both sides of the ordinate, and the angle  $\beta \geq \frac{\pi}{2}$  or  $\beta \leq \frac{\pi}{2}$  between the tangent equation at the center of mass and the abscissa gives

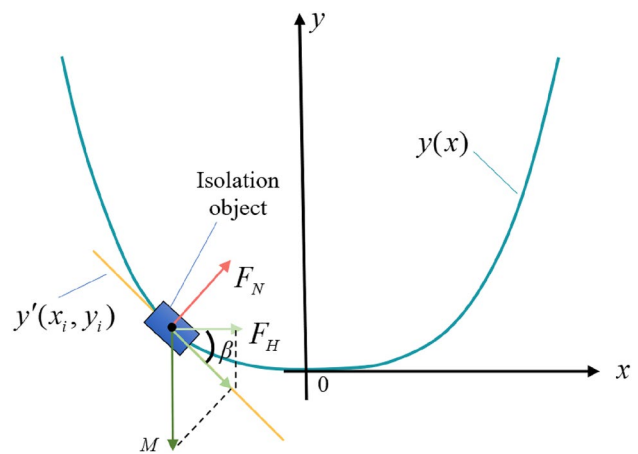


**Fig. 5** The force analysis model of a vibration isolated object

$$\beta = \arctan \left( y'_{(x_i, y_i)} \text{sign}(x_i) \right). \tag{13}$$

The horizontal restoring force of the isolating object is given by

$$F = M \sin(\beta) \cos(\beta). \tag{14}$$

The horizontal stiffness of the isolating object is given by

$$K = M(\cos^2(\beta) - \sin^2(\beta)). \tag{15}$$

As shown in Fig. 6, select three groups of vibration isolated objects whose masses are  $M_1 = 25$  kg,  $M_2 = 30$  kg, and  $M_3 = 35$  kg, respectively. Drawing force–displacement and stiffness–displacement curves, and observing the graph, it can be seen that the QZS characteristics of vibration isolators with different masses are more obvious the closer they are to the position of 0 within  $x \in (-0.04 \text{ m}, 0.04 \text{ m})$ . Thus, it can be concluded that the dynamic stiffness of vibration isolator can achieve QZS near the static equilibrium position.

### Dynamic Analysis

The horizontal restoring force obtained after the mechanical analysis of the vibration isolated object is relatively complicated, so the result of Taylor series expansion of the horizontal restoring force is  $F(x) = (15.5x^3 + 0.02x) \cdot M$ . The external horizontal acceleration excitation on the isolator base is  $-\Lambda \cos(\omega t)$ .  $M$  is the mass of the vibration isolated object (kg),  $z$  is the absolute displacement of the vibration isolation object (m),  $x$  is the relative displacement of the vibration isolation

object (m),  $c$  is the damping coefficient of the system (Ns/m), and  $F$  is the level resilience (N).

According to the vibration isolator model, the differential equation of motion of the working position is listed as follows:

$$M\ddot{x} + c\dot{x} + F = M\Lambda \cos \omega t. \tag{16}$$

Let  $\xi = \frac{c}{2\omega_0 M}$ ,  $\omega_0 = \frac{\omega}{\gamma}$ ,  $\tau = \omega_0 t$ , where  $\omega_0$  is the natural frequency of the system:

$$\ddot{x} + 2\xi\omega_0\dot{x} + \frac{F}{M} = \Lambda \cos \gamma \tau. \tag{17}$$

Since the horizontal restoring force  $F$  is a high-order function of relative displacement  $x$ , it is more complicated to use the traditional differential equation to solve it. According to the steady-state response of the system, the ordinary differential equation average method can be used to solve it.

Let the steady-state solution of the system be

$$x(\tau) = b(\tau) \cos(\gamma\tau + \theta(\tau)), \tag{18}$$

$$\dot{x}(\tau) = -b(\tau)\gamma \sin(\gamma\tau + \theta(\tau)). \tag{19}$$

The establishment of Eq. (19) should meet the following requirement:

$$\dot{b}(\tau) \cos(\gamma\tau + \theta(\tau)) - b(\tau)\dot{\theta}(\tau) \sin(\gamma\tau + \theta(\tau)) = 0. \tag{20}$$

In order to further solve the relationship between  $\dot{b}$  and  $\dot{\theta}$  variables, Eq. (20) is sorted out as follows:

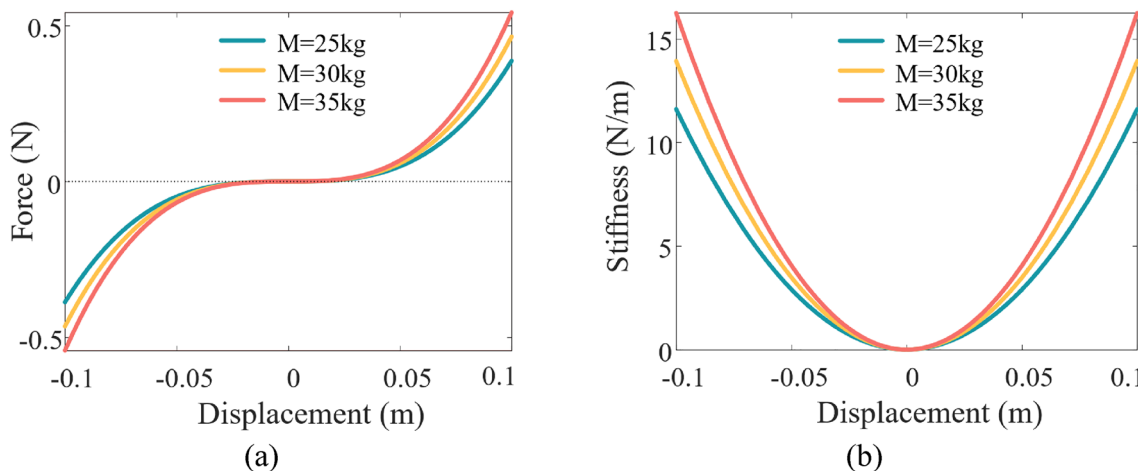


**Fig. 6** Force–displacement, stiffness–displacement curves. **a** Force–displacement curve, the horizontal component force value of the vibration isolation platform hardly changes within the horizontal dis-

placement  $(-0.04 \text{ m}, 0.04 \text{ m})$ , **b** the stiffness of the working platform of the isolator is close to 0 near the equilibrium position

$$\begin{cases} -b\gamma \sin(\gamma\tau + \theta) = -\frac{\dot{\theta}b\gamma \sin^2(\gamma\tau + \theta)}{\cos(\gamma\tau + \theta)} \\ -b\gamma\dot{\theta} \cos(\gamma\tau + \theta) = -\frac{b\gamma \cos^2(\gamma\tau + \theta)}{\sin(\gamma\tau + \theta)} \end{cases} \quad (21)$$

Equation (17) can be rewritten as

$$\begin{aligned} & -b\gamma \sin(\gamma\tau + \theta) - b\gamma^2 \cos(\gamma\tau + \theta) - b\gamma\dot{\theta} \cos(\gamma\tau + \theta) \\ & -2b\xi\gamma \sin(\gamma\tau + \theta) + 15.5b^3 \cos^3(\gamma\tau + \theta) + 0.02b \cos(\gamma\tau + \theta) = \Lambda \cos(\gamma\tau). \end{aligned} \quad (22)$$

Simplify Eqs. (21) and (22) to get

$$\begin{cases} \dot{\theta} = -\frac{1}{b\lambda} \Gamma \cos(\gamma\tau + \theta) \\ \dot{b} = -\frac{1}{\lambda} \Gamma \sin(\gamma\tau + \theta) \end{cases} \quad (23)$$

Here,

$$\begin{aligned} \Gamma = & b\gamma^2 \cos(\gamma\tau + \theta) + 2b\xi\omega_0\gamma \sin(\gamma\tau + \theta) - 15.5b^3 \cos^3(\gamma\tau + \theta) \\ & - 0.02b \cos(\gamma\tau + \theta) + \Lambda \cos(\gamma\tau). \end{aligned}$$

Let  $\beta = \gamma\tau + \theta$ , then

$$\Gamma = b\gamma^2 \cos \beta + 2b\xi\omega_0\gamma \sin \beta - 15.5b^3 \cos^3 \beta - 0.02b \cos \beta + \Lambda \cos(\beta - \theta).$$

In order to simplify the problem, take the average value of  $\dot{b}$  and  $\dot{\theta}$  within  $2\pi$  to replace its gradually changing real value, and rewrite the Eq. (23) to get

$$\begin{cases} \dot{\theta} = -\frac{1}{2\pi b\gamma} \int_0^{2\pi} \Gamma \cos \beta d\beta \\ \dot{b} = -\frac{1}{2\pi\gamma} \int_0^{2\pi} \Gamma \sin \beta d\beta \end{cases} \quad (24)$$

Solved:

$$\begin{cases} \dot{\theta} = -\frac{1}{2b\gamma} \left( b\gamma^2 - 0.02b - \frac{465b^3}{40} + \Lambda \cos \theta \right) \\ \dot{b} = -\frac{1}{2\gamma} (2b\xi\omega_0\gamma + \Lambda \sin \theta) \end{cases} \quad (25)$$

Let  $\dot{\theta} = 0$ ,  $\dot{b} = 0$  resolve to get

$$\begin{cases} b\gamma^2 - 0.02b - \frac{465b^3}{40} + \Lambda \cos \theta = 0 \\ 2b\xi\omega_0\gamma + \Lambda \sin \theta = 0 \end{cases} \quad (26)$$

Organized:

$$\Lambda^2 = \left( b\gamma^2 - 0.02b - \frac{465b^3}{40} \right)^2 + (2b\xi\omega)^2, \quad (27)$$

$$\cos \theta = \frac{-b\gamma^2 + 0.02b + \frac{465b^3}{40}}{\Lambda}. \quad (28)$$

The absolute displacement of the vibration isolated object is

$$z = \frac{\Lambda}{\omega^2} \cos \omega\tau + b \cos(\omega\tau + \theta) = \sqrt{b^2 + \frac{\Lambda}{\omega^2} + \frac{2\Lambda b}{\omega^2} \cos \theta} \sin(\omega\tau + \phi). \quad (29)$$

The absolute bit shift transmissibility is the ratio of the absolute displacement of the isolated object to the amplitude of the excitation displacement of the base:

$$T = \frac{\|z\|_{\max}}{\|y\|_{\max}} = \sqrt{1 + \frac{b^2\omega^4}{\Lambda^2} + \frac{2b\omega^2}{\Lambda^2} \left( -b\gamma^2 + 0.02b + \frac{465b^3}{40} \right)}. \quad (30)$$

Here,

$$\|y\|_{\max} = \sqrt{\frac{\Lambda^2}{\omega^4}},$$

$$\|z\|_{\max} = \sqrt{b^2 + \frac{\Lambda^2}{\omega^4} + \frac{2b}{\omega^2} \left( -b\gamma^2 + 0.02b + \frac{465b^3}{40} \right)}.$$

The displacement transmissibility of the vibration isolation system under different excitation amplitudes is shown in Fig. 7a. Other parameters are set to  $\omega = 1, \xi = 0.15$ . With the increase of excitation amplitude  $\Lambda$ , the peak value of transmissibility shifts to the right, and the peak value gradually increases. The onset frequency at which the isolator begins to isolate vibration has also increased. For example, when  $\Lambda$  increases from  $\Lambda=0.01$  to  $\Lambda=0.04$ , the starting frequency increases from 0.21 to 0.48, which means that the vibration isolation bandwidth becomes narrower. Furthermore, an increase in the excitation amplitude leads to a decrease in the vibration attenuation amplitude even in the isolation zone.

Figure 7b shows the displacement transfer rate under different damping ratios when the excitation amplitude  $\Lambda$  is 0.04. Increasing the damping ratio significantly reduces the peak transmissibility and suppresses the frequency jump phenomenon. But increasing the damping ratio  $\xi$  will reduce the vibration isolation performance of high-frequency vibration. Therefore, the consideration of damping in the vibration isolation system should be determined according to the actual working environment



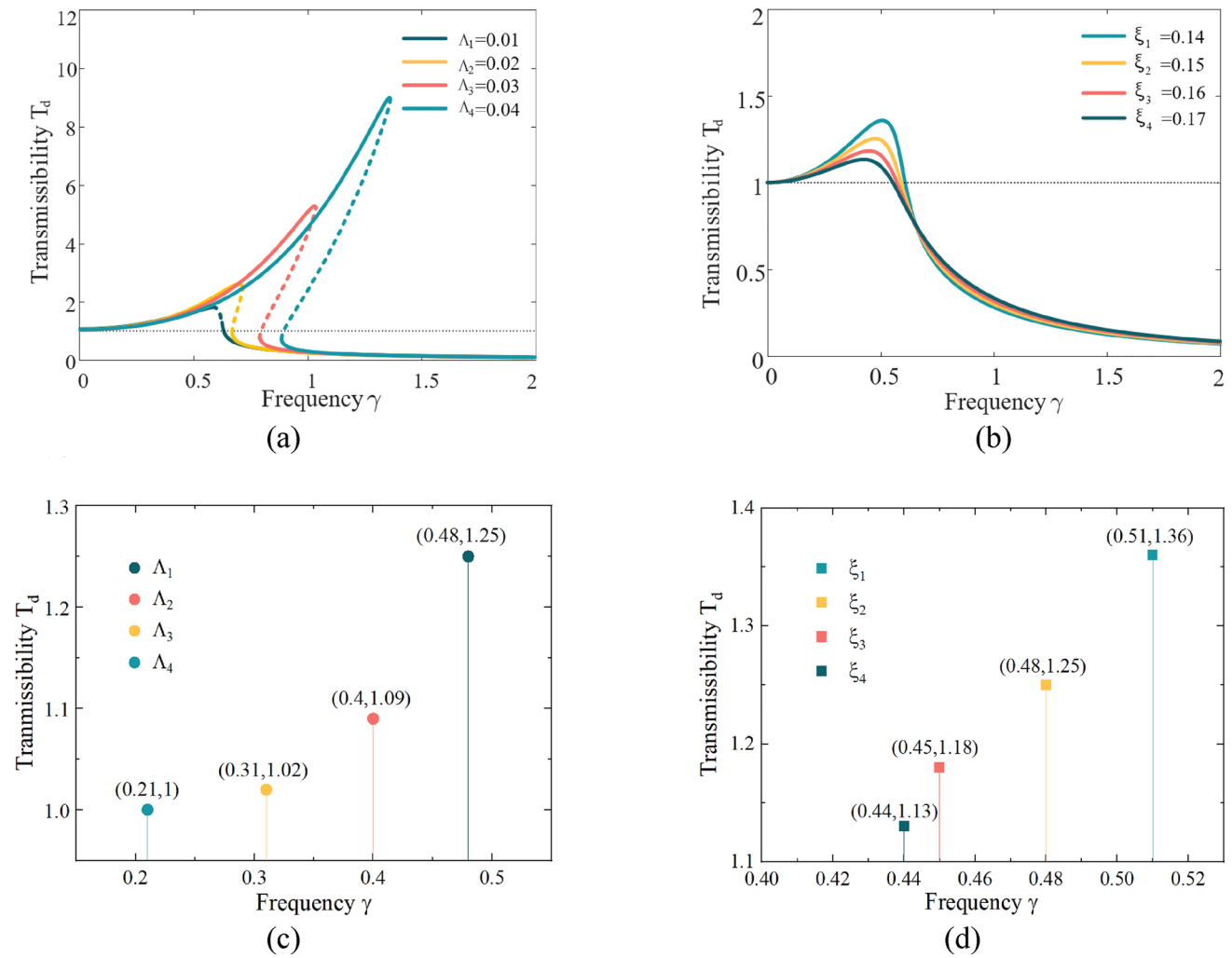


Fig. 7 Displacement transmissibility under different conditions

**Simulation Analysis of Vibration Isolation Effect**

The relevant kinematic pair constraint information is added to the simulation software and information such as rod density is set according to the optimized quality parameters. The dynamic and static friction factors of the Coulomb friction damping of the rotating pair are set to 0.012 and 0.02, respectively. When the disturbance input  $\Lambda \cos(\omega t)$ , the simulation results are shown in Fig. 8.

It can be seen from Fig. 8a that the vibration isolator has good vibration isolation effect under different load masses under the disturbance of the external simple harmonic excitation frequency of 4 Hz, and the greater the mass, the better the vibration isolation effect. It can be seen from Fig. 8b that the vibration amplitude of the vibration isolator is attenuated by 90.2% under the external harmonic excitation frequency of 8 Hz. When the mass of the vibration isolator increases exponentially, the

simulation results under the three conditions show that the vibration isolation attenuation does not change proportionally, and the difference in the simulation results is small, which indicates that the vibration isolation performance of the vibration isolator has little correlation with the load mass. Therefore, the vibration isolator can meet the low-frequency horizontal vibration isolation requirements with large external disturbance amplitude.

**Experimental Validation**

In this section, an experimental model is established to test the force–displacement relationship corresponding to loads of different masses. In addition, the dynamic test is

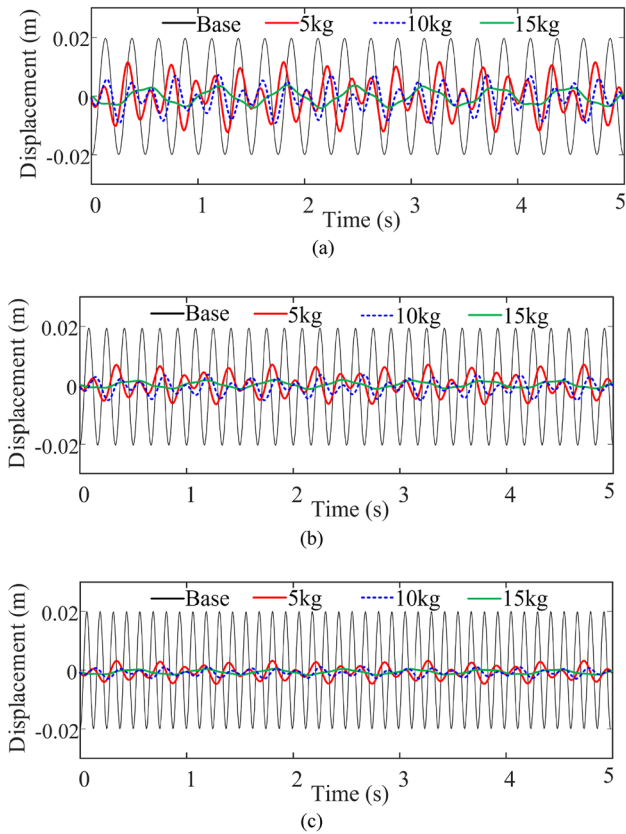


**Fig. 8** The absolute displacement of the working platform and base when the vibration isolator is excited periodically at different frequencies: **a**  $\omega = 8\pi$ , **b**  $\omega = 12\pi$ , **c**  $\omega = 16\pi$  when  $\Lambda = 0.02$  m

performed to evaluate the vibration isolation performance of the dual four-rod horizontal isolators.

### Resilience Test

As shown in Fig. 9, the experimental prototype of the vibration isolator is placed on the horizontal platform, and multiple groups of loads with different masses are selected and fixed on the working platform of the vibration isolator. The tension sensor is used to measure the horizontal restoring force of the load, one end of which is connected to the center of the working platform of the vibration isolator and the other end is fixed on the horizontal platform. The initial position of the load is selected at 0.04 m on the negative axis of the abscissa, and a total of 20 data points are selected within  $(-0.04 \text{ m}, 0.04 \text{ m})$ , and the values of the restoring force and corresponding displacement are recorded and the experimental data are plotted in a point diagram. As shown in Fig. 10, the experimental data is in good agreement with

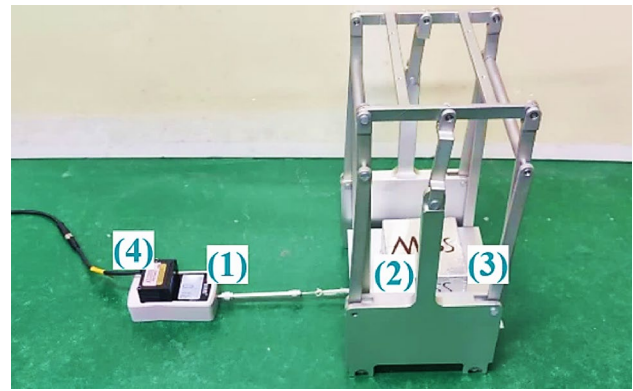


**Fig. 9** Resilience test. (1) Digital tension gauge (XDS-10), (2) load, (3) working platform, (4) intelligent-L laser sensor (IL-100)

the theoretical data, indicating that the experimental prototype of the vibration isolator satisfies the QZS characteristic near the static equilibrium position.

### Transmissibility Experiment

In order to further verify the frequency response characteristics and transmissibility of the vibration isolator, and evaluate the accuracy of theoretical analysis and dynamic simulation results, this section conducts vibration test experiments on the vibration isolator. The vibration isolation performance test system is shown in Fig. 11. The drive controller (CMba2B04N0N800WNNNYN) outputs control signals to control the movement of the vibration table (CDL40001-00). Two acceleration sensors (AI050) are, respectively, fixed on the base of the vibration isolator and the working platform, one is used to measure the excitation acceleration, and the other is used to measure the response acceleration of the load. A dynamic signal analyzer (JM5936) simultaneously collects signals from two accelerometers and transmits them to a computer (Dell).

The frequency of periodic excitation ranges from 4 to 10 Hz, and the amplitude of each periodic displacement excitation is set to 0.02 m. When the excitation frequencies are, respectively, 4 Hz, 6 Hz, 8 Hz and 10 Hz, the time-domain acceleration results of the base and the working platform are shown in Fig. 12. The acceleration of the base is less than that of the working platform, which means that the vibration of the base is effectively attenuated. The greater the excitation frequency, the greater the attenuation is. Acceleration transmissibility is defined by the ratio of the acceleration amplitude of the working platform to that of the base. For example, when the excitation frequency is 8 Hz,

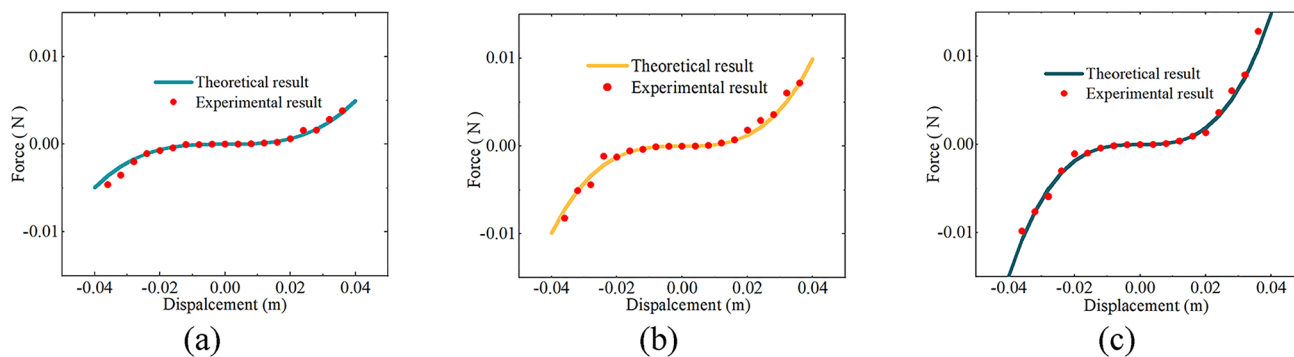


**Fig. 10** Force–displacement diagrams of theoretical and experimental results under different loads: **a** 5 kg, **b** 10 kg, **c** 15 kg

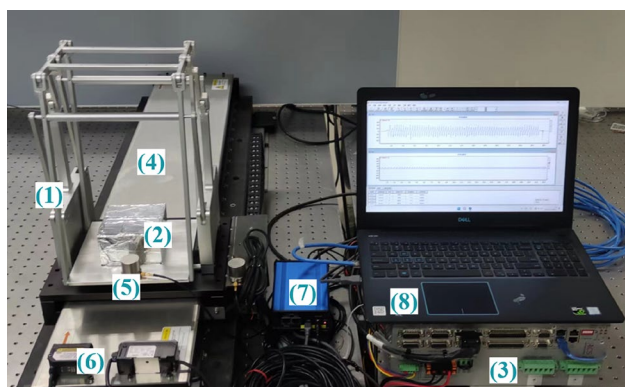


**Fig. 11** Dynamics experiment in which: (1) experimental model of shock isolator, (2) load, (3) ACS motion control, (4) shaking table, (5) acceleration sensor, (6) laser range finder (IL-100), (7) dynamic analyzer, (8) computer

the acceleration of the base of the isolator is  $50.52 \text{ mm/s}^2$ , the acceleration of the working platform is  $6.1 \text{ mm/s}^2$ , and the vibration of the base is attenuated by about 87.9%. The change of acceleration transitivity with excitation frequency under periodic excitation is shown in Fig. 13. The vibration isolator starts to work at  $\omega = 2.1 \text{ Hz}$ , and with the increase in frequency, the isolation effect becomes more and more obvious. In addition, the experimental transfer rate is in good agreement with the theoretical transfer rate.

### Conclusions

A new dual four-rod horizontal large-amplitude QZS vibration isolator is proposed, which draws on the structural singularity of planar linkage mechanism under special configuration. The vibration isolation performance is improved

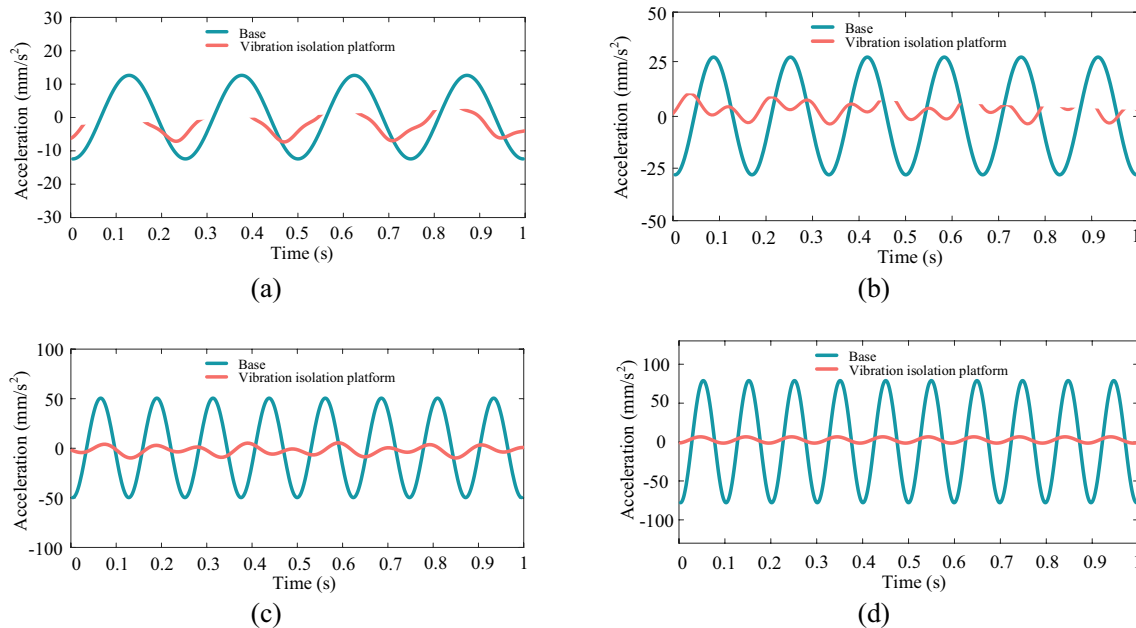


**Fig. 12** Acceleration of platform and base under periodic excitation with different frequencies: **a** 4 Hz, **b** 6 Hz, **c** 8 Hz, **d** 10 Hz

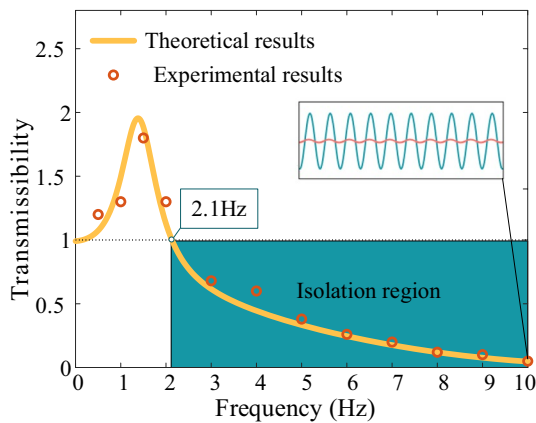


**Fig. 13** Acceleration transfer rate of the isolator under excitation with a periodic frequency of 1–10 Hz

by realizing the QZS characteristic in the static equilibrium position, and the QZS range is expanded by parameter optimization design. The static analysis of the vibration isolator is carried out. By optimizing the rod length parameters, the motion trajectory of the vibration isolator near the equilibrium position is horizontal quasi-straight line, and the position of the equivalent centroid is stable. After optimization, the stiffness curve increases the QZS range, and the dynamic stiffness is lower in the whole vibration isolation range. Through the analysis of harmonic excitation and transmission rate, the results show that the isolator has lower resonance peak value, lower initial isolation frequency and wider isolation bandwidth. The physical prototype of the isolator is made and the experimental platform is built. The isolation performance of the isolator is evaluated through the isolation performance tests under different frequency external excitation. The results show that the isolator can effectively isolate the external excitation greater than 3 Hz.

**Author Contributions** Conceptualization, SW, LY, QZ and RX; methodology, SW, LY and QZ; software, SW and LY; validation, SW and LY; investigation, SW, QZ; data curation, SW, LY and QZ; writing—original draft preparation, SW and LY; writing—review and editing, SW, LY and QZ; visualization, SW; supervision, QZ, RX; project administration, QZ, RX; funding acquisition, QZ. All the authors have read and agreed to the published version of the manuscript.

**Funding** This research was funded by the National Natural Science Foundation, China (Grant no. 52105009), by the Project of Shenzhen Municipal Science and Technology Innovation Council (Grant no. KCXFZ20201221173202007), by the Key Scientific Research Platforms and Projects of Guangdong Regular Institutions of Higher Education, China (Grant no. 2022KCXTD033), by the Scientific Research Capacity Improvement Project of Key Developing Disciplines in Guangdong Province, China (Grant no. 2021ZDJS084), by the Guangdong Natural Science Foundation, China (Grant no. 2023A1515012103), by the Key Laboratory of Robotics and

Intelligent Equipment of Guangdong Regular Institutions of Higher Education, China (Grant no. 2017KSYS009), and by the Innovation Center of Robotics and Intelligent Equipment, China (Grant no. KCYCXPT2017006).

**Availability of Data and Materials** The data used to support the findings of this study are included within the article.

**Code Availability** Not applicable.

## Declarations

**Conflict of Interest** The authors declare that there is no conflict of interest.

**Ethics Approval** Not applicable.

**Consent to Participate** Not applicable.

**Consent for Publication** Not applicable.

## References

- Zou W, Cheng C, Ma R et al (2021) Performance analysis of a quasi-zero stiffness vibration isolation system with scissor-like structures[J]. *Arch Appl Mech* 91:117–133
- Yan B, Yu N, Ma H et al (2022) Crosspolar variations on a satellite-Earth path[J]. *Mech Syst Signal Process* 167:108507
- Li M, Cheng W, Xie R (2020) Design and experiments of a quasi-zero-stiffness isolator with a noncircular cam-based negative-stiffness mechanism[J]. *J Vib Control* 26(21–22):1935–1947
- Martínez-Pañeda E, Fleck NA (2018) Crack growth resistance in metallic alloys: the role of isotropic versus kinematic hardening[J]. *J Appl Mech* 85(11):111002
- Sadeghi S, Li S (2019) Fluidic origami cellular structure with asymmetric quasi-zero stiffness for low-frequency vibration isolation[J]. *Smart Mater Struct* 28(6):065006
- Ledezma-Ramírez DF, Tapia-González PE, Ferguson N et al (2019) Recent advances in shock vibration isolation: An overview and future possibilities[J]. *Appl Mech Rev* 71(6):060802
- Ding H, Ji J, Chen LQ (2019) Nonlinear vibration isolation for fluid-conveying pipes using quasi-zero stiffness characteristics[J]. *Mech Syst Signal Process* 121:675–688
- Ye K, Ji JC (2022) An origami inspired quasi-zero stiffness vibration isolator using a novel truss-spring based stack Miura-ori structure[J]. *Mech Syst Signal Process* 165:108383
- Abuabiah M, Dabbas Y, Herzallah L et al (2022) Analytical study on the low-frequency vibrations isolation system for vehicle's seats using quasi-zero-stiffness isolator[J]. *Appl Sci* 12(5):2418
- Yan G, Zou HX, Wang S et al (2022) Bio-inspired toe-like structure for low-frequency vibration isolation[J]. *Mech Syst Signal Process* 162:108010
- Zhang Q, Guo D, Hu G (2021) Tailored mechanical metamaterials with programmable quasi-zero-stiffness features for full-band vibration isolation[J]. *Adv Func Mater* 31(33):2101428
- Carrella A, Brennan MJ, Kovacic I et al (2009) On the force transmissibility of a vibration isolator with quasi-zero-stiffness[J]. *J Sound Vib* 322(4–5):707–717
- Xu D, Zhang Y, Zhou J et al (2014) On the analytical and experimental assessment of the performance of a quasi-zero-stiffness isolator[J]. *J Vib Control* 20(15):2314–2325

14. Lan CC, Yang SA, Wu YS (2014) Design and experiment of a compact quasi-zero-stiffness isolator capable of a wide range of loads[J]. *J Sound Vib* 333(20):4843–4858
15. Bouna HS, Nbandjo BRN, Wofo P (2020) Isolation performance of a quasi-zero stiffness isolator in vibration isolation of a multi-span continuous beam bridge under pier base vibrating excitation[J]. *Nonlinear Dyn* 100:1125–1141
16. Zhao F, Cao S, Luo Q et al (2022) Practical design of the QZS isolator with one pair of oblique rods by considering pre-compression and low-dynamic stiffness[J]. *Nonlinear Dyn* 108(4):3313–3330
17. Alabuzhev P, Gritchin KL et al (1989) *Vibration protecting and measuring systems with quasi-zero-stiffness*[M]. Hemisphere Publishing Corporation, London, pp 7–21
18. Carrella A, Brennan MJ, Waters TP (2007) Static analysis of a passive vibration isolator with quasi-zero-stiffness characteristic[J]. *J Sound Vib* 301(3–5):678–689
19. Carrella A, Brennan MJ, Waters TP et al (2012) Force and displacement transmissibility of a nonlinear isolator with high-static-low-dynamic-stiffness[J]. *Int J Mech Sci* 55(1):22–29
20. Kovacic I, Brennan MJ, Waters TP (2008) A study of a nonlinear vibration isolator with a quasi-zero stiffness characteristic[J]. *J Sound Vib* 315(3):700–711
21. Zhou J, Wang X, Xu D et al (2015) Nonlinear dynamic characteristics of a quasi-zero stiffness vibration isolator with cam–roller–spring mechanisms[J]. *J Sound Vib* 346:53–69
22. Kim J, Jeon Y, Um S et al (2019) A novel passive quasi-zero stiffness isolator for ultra-precision measurement systems[J]. *Int J Precis Eng Manuf* 20:1573–1580
23. Dalela S, Balaji PS, Jena DP (2022) Design of a metastructure for vibration isolation with quasi-zero-stiffness characteristics using bistable curved beam[J]. *Nonlinear Dyn* 108(3):1931–1971
24. Zhang C, Li X, Zhang S et al (2022) Design and analysis of quasi-zero stiffness torsional vibration isolator adapting to load changes[J]. *J Vib Shock* 41(23):307–314
25. Zhou X, Sun X, Zhao D et al (2021) The design and analysis of a novel passive quasi-zero stiffness vibration isolator[J]. *J Vib Eng Technol* 9(2):225–245
26. Liu X, Zhao Q, Zhang Z et al (2019) An experiment investigation on the effect of coulomb friction on the displacement transmissibility of a quasi-zero stiffness isolator[J]. *J Mech Sci Technol* 33:121–127
27. Burian YA, Silkov MV, Sitnikov DV (2020) Quasi-zero stiffness vibration isolation support with stiffness corrector based on a rubber-cord air spring[C]. *AIP Conf Proc AIP Publ LLC* 2285(1):030007
28. Cai C, Zhou J, Wu L et al (2020) Design and numerical validation of quasi-zero stiffness metamaterials for very low-frequency band gaps[J]. *Compos Struct* 236:111862
29. Zhou J, Pan H, Cai C et al (2021) Tunable ultralow frequency wave attenuations in one-dimensional quasi-zero stiffness metamaterial[J]. *Int J Mech Mater Des* 17:285–300
30. Xing ZY, Yang XD (2023) A combined vibration isolation system with quasi-zero stiffness and dynamic vibration absorber[J]. *Int J Mech Sci* 256:108508
31. Zeng R, Wen G, Zhou J et al (2021) Limb-inspired bionic quasi-zero stiffness vibration isolator[J]. *Acta Mech Sin* 37(7):1152–1167
32. Chai Y, Jing X, Guo Y (2022) A compact X-shaped mechanism based 3-DOF anti-vibration unit with enhanced tunable QZS property[J]. *Mech Syst Signal Process* 168:108651
33. Ling P, Miao L, Ye B et al (2023) Ultra-low frequency vibration isolation of a novel click-beetle-inspired structure with large quasi-zero stiffness region[J]. *J Sound Vib* 558:117756

**Publisher's Note** Springer Nature remains neutral with regard to jurisdictional claims in published maps and institutional affiliations.

Springer Nature or its licensor (e.g. a society or other partner) holds exclusive rights to this article under a publishing agreement with the author(s) or other rightsholder(s); author self-archiving of the accepted manuscript version of this article is solely governed by the terms of such publishing agreement and applicable law.